Attenuation analysis for heterogeneous transversely isotropic media

Bharath Shekar & Ilya Tsvankin
Center for Wave Phenomena, Colorado School of Mines, Golden CO 80401

ABSTRACT
Attenuation coefficients obtained from seismic data may provide sensitive attributes for reservoir characterization and increase the robustness of AVO (amplitude variation with offset) analysis. Here, we present an algorithm for ray tracing in attenuative anisotropic media based on the methodology of Červený and Pšenčik. Both kinematic and dynamic ray tracing are carried out in an elastic reference medium, with the attenuation terms incorporated as perturbations along the ray. Numerical examples for smoothly varying transversely isotropic (TI) media demonstrate the accuracy of the method.
The dynamic ray-tracing technique provides an efficient forward-modeling operator that can be used in the inversion for anisotropic attenuation. We outline an inversion methodology for estimating attenuation coefficients in 2D heterogeneous anisotropic media. A necessary prerequisite for accurate attenuation analysis is reconstruction of the heterogeneous velocity field. If the subsurface can be approximated by a piecewise-factorized VTI (TI with a vertical axis of symmetry) medium, the anisotropic velocity model can be built using the migration velocity analysis algorithm proposed by Sarkar and Tsvankin. Attenuation coefficients in each factorized block can then be estimated using gradient-based inversion that employs dynamic ray tracing.

Introduction

Seismic attenuation is sensitive to lithology and physical properties of subsurface rocks (Johnston and Toksöz, 1981), so it can provide valuable attributes for reservoir characterization (Lynn, 2004). Compensation for attenuation also helps improve the quality of images obtained by depth migration (e.g., Xin et al., 2008).

The amplitudes of seismic waves are determined by the source characteristics and medium properties including velocity, attenuation coefficients, density, etc. In addition to attenuation, dynamic signatures are influenced by a variety of propagation phenomena including reflection, transmission, mode conversions, triplications, focusing, scattering by heterogeneities, etc. In surface seismic surveys, such factors as source and receiver coupling and near-surface heterogeneities can further distort recorded amplitudes.

Hence, estimation of attenuation from surface seismic data is a challenging problem, and stable attenuation analysis typically requires the subsurface structure to be relatively simple. Brzostowski and McMechan (1992) propose a tomographic algorithm that relies on the spectral-ratio method (Johnston and Toksöz, 1981) to compute isotropic attenuation coefficients from a field data set. They first estimate the 3D velocity structure and then use the simultaneous iterative reconstruction technique (SIRT) (Menke, 1984) to invert for attenuation. While the results are satisfactory for the shallow layers, they deteriorate with depth. The centroid frequency shift method is utilized by Quan and Harris (1997) to construct isotropic attenuation tomograms from a cross-hole data set acquired in West Texas field. Liao and McMechan (1997) apply the same method to a cross-hole survey from Oklahoma to discriminate between sands and shales based on the isotropic attenuation coefficients.

Zhu et al. (2007) extend the spectral-ratio method to anisotropic media and estimate angle-dependent attenuation coefficients from physical-modeling data. Behura and Tsvankin (2009a) introduce a layer-stripping algorithm that combines the velocity-independent layer stripping (VILS) method of Dewangan and Tsvankin (2006) with the spectral-ratio technique to estimate interval attenuation coefficients of pure (PP or SS) reflected waves. The overburden is assumed to be laterally homogeneous (but possibly vertically heterogeneous) with a horizontal symmetry plane, while the target layer may be arbitrarily anisotropic and heterogeneous. By matching time slopes on common-receiver gathers, Behura and Tsvankin (2009a) identify the overburden and target events that share ray segments in the overburden and compute the interval traveltime and then the inter-

val attenuation coefficient in the target horizon. Reine et al. (2009) propose a similar layer-stripping algorithm to evaluate interval P-wave attenuation in anisotropic media. Since their method operates in the $\tau - p$ domain, it is restricted to laterally homogeneous target layers.

Shekar and Tsvankin (2011) extend the attenuation layer-stripping method of Behura and Tsvankin (2009a) to mode-converted (PS) waves with the goal of estimating the interval S-wave attenuation coefficient. By identifying PP and PS events with shared ray segments and applying the PP+PS=SS method, they first perform kinematic construction of pure shear (SS) events in the target layer and overburden. Then, the effective shear-wave attenuation coefficients for the overburden and target reflections are obtained from the modified spectral-ratio method. Finally, the dynamic version of VILS is used to compute the S-wave interval attenuation coefficient in the target layer.

The attenuation layer-stripping method, however, is restricted to models with a laterally homogeneous overburden. Here, we build the foundation for extending attenuation analysis to transversely isotropic models with spatially varying velocity and attenuation functions. First, we review the perturbation method of Červený and Pšenčik (2009) for dynamic ray tracing in anisotropic, attenuative media and implement it for heterogeneous TI models. Then we present numerical examples for homogeneous and smoothly varying 2D TI media to verify the accuracy of the algorithm in modeling P-wave attenuation. We conclude by introducing a strategy to invert reflection data for attenuation coefficients in piecewise-factorized VTI media.

Modeling of seismic wave propagation in attenuative media

In attenuative media, the stiffness tensor becomes complex, which leads to amplitude decay along seismic rays and velocity dispersion. The time-domain stiffness tensor is called the relaxation tensor, and stress is obtained by convolving the relaxation tensor with the strain tensor (Carcione, 1990), which complicates time-domain finite-difference modeling of seismic wave propagation. Further, to simulate frequency-independent attenuation ("constant-Q" model, e.g., Kjartannson, 1979) it is essential to superimpose various relaxation mechanisms in both isotropic (Xu and McMechan, 1998) and anisotropic (Ruud and Hestholm, 2005) media, thus increasing the cost of finite-difference modeling. Although the approach proposed by Carcione (2011) based on the Fourier pseudospectral method avoids the computation of relaxation functions, it is limited to viscoacoustic media. The reflectivity method (Schmidt and Tango, 1986) can also be used to calculate exact synthetic seismograms in 1D attenuative media. However, it is restricted to laterally homogeneous models with flat interfaces, and not suitable for our purposes.

Therefore, here we compute asymptotic Green's functions in attenuative anisotropic media using dynamic ray tracing (Červený, 2001). So-called "complex" ray theory treats ray trajectories and parameters computed along the ray as complex quantities (Thomson, 1997; Hanyga and Seredyńska, 2000). However, numerical implementation of "complex" ray theory for seismic applications is not straightforward. Alternatively, ray tracing in attenuative media can be performed using perturbation methods (Gajewski and Pšenčik, 1992; Červený and Pšenčik, 2009), which involves computation of rays in a reference elastic medium with the influence of attenuation modeled as a perturbation along the ray.

Next, we briefly review the ray-tracing methodology of Červený and Pšenčik (2009) which enables the calculation of the asymptotic Green's function in attenuative, anisotropic, heterogeneous media with smooth spatial variations of the stiffness tensor.

Dynamic ray tracing in elastic media

The eikonal equation in elastic, anisotropic, heterogeneous media can be written as:

$$\mathcal{H}(x_a, p_b) = \frac{1}{2}\,[G_m(x_a, p_b)], \tag{1}$$

where $\mathcal{H}$ is the Hamiltonian and x_a and p_b denote the spatial Cartesian coordinates and components of the slowness vector, respectively. No summation is implied over indices a and b. The term $G_m(x_a, p_b)$ denotes an eigenvalue of the Christoffel matrix.

Hereafter, we consider in-plane polarized waves in a vertical (x-z) plane of VTI media, so a, b and all the other Roman indices take the values 1 and 3. The subscript m in $G_m(x_a, p_b)$ will be omitted, and the eigenvalue will be assumed to correspond to P-waves. The Christoffel matrix is given by

$$\Gamma_{ik}(x_a, p_b) = a_{ijkl}(x_a)\, p_j\, p_l, \tag{2}$$

where a_{ijkl} is the density-normalized stiffness tensor. Summation over indices $j = 1, 3$ and $l = 1, 3$ is implied; $i = 1, 3$ and $k = 1, 3$. The eigenvalue of the Christoffel matrix is formally written as

$$G(x_a, p_b) = g_i\, a_{ijkl}\, p_j\, p_l\, g_k, \tag{3}$$

where the components g_i form the unit polarization vector.

The kinematic ray-tracing equations are given by:

$$\frac{\mathrm{d}x_i}{\mathrm{d}\tau} = \frac{\partial \mathcal{H}}{\partial p_i}, \tag{4}$$

$$\frac{\mathrm{d}p_i}{\mathrm{d}\tau} = -\frac{\partial \mathcal{H}}{\partial x_i}, \tag{5}$$

with the Hamiltonian $\mathcal{H}$ defined in equation 1; τ represents the traveltime (eikonal) along the ray. Dynamic

ray tracing is performed by solving the following equations:

$$\frac{\mathrm{d}Q_{ia}}{\mathrm{d}\tau} = \frac{\partial^2\mathcal{H}}{\partial p_i \partial x_j}\, Q_{ja} + \frac{\partial^2\mathcal{H}}{\partial p_i \partial p_j}\, P_{ja}, \tag{6}$$

$$\frac{\mathrm{d}P_{ia}}{\mathrm{d}\tau} = -\frac{\partial^2\mathcal{H}}{\partial x_i \partial x_j}\, Q_{ja} - \frac{\partial^2\mathcal{H}}{\partial p_j \partial x_j}\, P_{ja}. \tag{7}$$

The matrices $\mathbf{Q}$ and $\mathbf{P}$ are defined as:

$$Q_{i1} = \frac{\partial x_i}{\partial \gamma_1}, \quad Q_{i3} = \frac{\partial x_i}{\partial \tau}, \tag{8}$$

$$P_{i1} = \frac{\partial p_i}{\partial \gamma_1}, \quad P_{i3} = \frac{\partial x_i}{\partial \tau}, \tag{9}$$

where γ_1 is a ray parameter (e.g., the phase take-off angle). The initial conditions for a point source are specified in Moser and Červený (2009).

Dynamic ray tracing in viscoelastic media

The density-normalized stiffness tensor for attenuative media is complex-valued:

$$\tilde{a}_{ijkl} = a^R_{ijkl} + \mathrm{i}\, a^I_{ijkl}, \tag{10}$$

where a^R_{ijkl} and a^I_{ijkl} are the real and imaginary parts of $\tilde{a}$. The ray-theoretical frequency-domain displacement of P-waves propagating in heterogeneous, attenuative, anisotropic media has the form:

$$\mathbf{u}(x_a,\omega) = S(\omega)\,\mathbf{A}(x_a)\,\exp[-\mathrm{i}\,\omega(t - \mathrm{Re}\,\tau(x_a)] \cdot \exp[-\omega\,\mathrm{Im}\,\tau(x_a)], \tag{11}$$

where $\mathbf{u}(x_a,\omega)$ is the displacement vector, $S(\omega)$ is the source spectrum, $\mathbf{A}(x_a)$ (assumed to be frequency-independent) incorporates the geometrical spreading and transmission coefficients along the raypath, the polarization vector, and the source/receiver directivity. The real and imaginary parts of the traveltime $\tau(x_a)$ contribute to the phase and amplitude functions along the ray, respectively. The imaginary part of the traveltime is often called the "dissipation factor" and denoted by t^* (Gajewski and Pšenčík, 1992):

$$t^*(x_a) = \mathrm{Im}\,\tau(x_a). \tag{12}$$

The factor responsible for the exponential amplitude decay is called the dissipation filter $D(\omega)$:

$$D(\omega) = \exp[-\omega\, t^*(x_a)]. \tag{13}$$

Červený and Pšenčík (2009) show that for weakly attenuative media, it is sufficient to perform dynamic ray tracing in the reference medium using equations 4–9. The complex traveltime can be computed as a perturbation of the real-valued traveltime found along the ray. The density-normalized stiffnesses a^R_{ijkl} correspond to the reference medium, and the term a^I_{ijkl} is the perturbation that makes the medium viscoelastic. Červený and Pšenčík (2009) define the perturbation Hamiltonian $\mathcal{H}(x_a,p_b,\alpha)$ as follows:

$$\mathcal{H}(x_a,p_b,\alpha) = \mathcal{H}^0(x_a,p_b) + \alpha\,\triangle\mathcal{H}(x_a,p_b), \tag{14}$$

with

$$\triangle\mathcal{H}(x_a,p_b) = \tilde{\mathcal{H}}(x_a,p_b) - \mathcal{H}^0(x_a,p_b), \tag{15}$$

where $\mathcal{H}^0$ and $\tilde{\mathcal{H}}$ correspond to the (elastic) reference and (viscoelastic) perturbed medium, respectively, and α is the perturbation parameter. The Hamiltonian $\mathcal{H}^0$ can be expressed through the slowness ($\mathbf{p}$) and polarization ($\mathbf{g}$) vectors computed for the reference medium:

$$\mathcal{H}^0(x_a,p_b) = \frac{1}{2}\left[g_i\, a_{ijkl}\, p_j\, p_l\, g_k\right], \tag{16}$$

and $\tilde{\mathcal{H}}$ is given by

$$\tilde{\mathcal{H}}(x_a,p_b) = \frac{1}{2}\left[\tilde{g}^*_i\,(a^R_{ijkl} + \mathrm{i}\, a^I_{ijkl})\, p_j\, p_l\, \tilde{g}_k\right], \tag{17}$$

where the polarization vector $\tilde{\mathbf{g}}$ computed for the perturbed medium is complex and the asterisk denotes the complex conjugate. The vector $\tilde{\mathbf{g}}$ is found as the eigenvector of the perturbed Christoffel matrix $\tilde{\Gamma}_{ik}$:

$$\tilde{\Gamma}_{ik} = (a^R_{ijkl} + \mathrm{i}\, a^I_{ijkl})\, p_j\, p_l, \tag{18}$$

and it satisfies the condition

$$\tilde{\mathbf{g}}\,.\,\tilde{\mathbf{g}}^* = 1. \tag{19}$$

The traveltime $\tau(x_a,\alpha)$ and its spatial derivatives $\partial\tau(x_a,\alpha)/\partial x_i$, which correspond to the perturbation Hamiltonian defined in equation 14, can be expanded in the perturbation parameter α:

$$\tau(x_a,\alpha) \approx \tau(x_a) + \alpha\,\frac{\partial\tau(x_m,\alpha)}{\partial\alpha} + \frac{1}{2}\,\alpha^2\,\frac{\partial^2\tau(x_a,\alpha)}{\partial\alpha^2}, \tag{20}$$

$$\frac{\partial\tau(x_a,\alpha)}{\partial\alpha} \approx \frac{\partial\tau_\alpha(x_a)}{\partial x_i} + \alpha\,\frac{\partial^2\tau(x_a,\alpha)}{\partial x_i\partial\alpha}, \tag{21}$$

where $\tau(x_a)$ and $\partial\tau(x_a)/\partial x_i$ correspond to the reference medium. The partial derivatives in equations 20 and 21 are computed as quadratures along the ray using the reference and perturbation Hamiltonians defined in equations 14–17, and are evaluated for $\alpha = 0$.

Equations 20 and 21 can be separated into the real and imaginary part:

$$\tau(x_a,\alpha) = \mathrm{Re}\,\tau(x_a,\alpha) + \mathrm{i}\,\mathrm{Im}\,\tau(x_a,\alpha), \tag{22}$$

$$\frac{\partial\tau(x_a,\alpha)}{\partial x_i} = \mathrm{Re}\,\frac{\partial\tau(x_a,\alpha)}{\partial x_i} + \mathrm{i}\,\mathrm{Im}\,\frac{\partial\tau(x_a,\alpha)}{\partial x_i}. \tag{23}$$

The dissipation factor and its spatial gradient in the perturbed attenuative medium can be found by substituting $\alpha = 1$ into equations 20 and 21 and using equations 12, 22, and 23:

$$t^*(x_a) = \mathrm{Im}\,\tau(x_a) \approx \mathrm{Im}\,\tau_{,\alpha}(x_m) + \frac{1}{2}\,\tau_{,\alpha\alpha}(x_a), \tag{24}$$

$$t^*_{,x_i}(x_a) = \mathrm{Im}\,\tau_{,x_i}(x_a) \approx \mathrm{Im}\,\tau_{,x_i\,\alpha}(x_a), \qquad (25)$$

where $\tau_{,\alpha} = \partial\tau/\partial\alpha$, $\tau_{,x_i} = \partial\tau/\partial x_i$, $\tau_{,\alpha\alpha} = \partial^2\tau/\partial\alpha^2$ and $\tau_{,\alpha x_i} = \partial^2\tau/(\partial\alpha\,\partial x_i)$.

The P-wave phase attenuation coefficient $\mathcal{A}_P$ is defined as

$$\mathcal{A}_P = \frac{k^I}{k^R}, \qquad (26)$$

where k^R and k^I are the real and imaginary parts of the wave vector, respectively. The local group attenuation coefficient at any point in space x_a is given by

$$\mathcal{A}_P(x_a) = -\mathrm{Im}\,\tilde{\mathcal{H}}(x_a) = \frac{1}{2Q(x_a)}, \qquad (27)$$

where $Q(x_a)$ is defined as the local quality factor. Červený and Pšenčik (2009) prove that equation 27 produces the phase attenuation coefficient computed in the phase direction corresponding to the ray (or to the group angle), and that it is not influenced by the inhomogeneity angle (the angle between the real and imaginary parts of the wave vector). This result agrees with the general perturbation analysis of the influence of the inhomogeneity angle presented by Behura and Tsvankin (2009b).

The exact phase attenuation coefficient in TI media can be found by solving the complex Christoffel equation (Červený and Pšenčik, 2005; Zhu and Tsvankin, 2006). Zhu and Tsvankin (2006) also present the following linearized approximation for the P-wave phase attenuation coefficient under the assumptions of weak attenuation and weak velocity and attenuation anisotropy:

$$\mathcal{A}_P(\theta) = \mathcal{A}_{P0}\,(1 + \delta_Q \sin^2\theta\cos^2\theta + \epsilon_Q \sin^4\theta), \qquad (28)$$

where $\mathcal{A}_{P0} = 1/(2Q_{P0})$ is the P-wave symmetry-direction attenuation coefficient and θ is the phase angle with the symmetry axis. The attenuation-anisotropy parameters ϵ_Q and δ_Q depend on the ratios of the real and imaginary parts of the stiffness coefficients and on the velocity-anisotropy parameters (Zhu and Tsvankin, 2006; Tsvankin and Grechka, 2011). We use both the exact and linearized attenuation coefficient in the synthetic examples below.

Numerical examples

To test the algorithm described above, we consider an anisotropic halfspace with smoothly varying velocity and attenuation parameters. The velocity parameters ϵ and δ and attenuation-anisotropy parameters ϵ_Q and δ_Q are constant, while the P-wave vertical velocity V_{P0} and vertical quality factor Q_{P0} vary as linear functions of the spatial coordinates:

$$V_{P0}(x,z) = V^{(0)}_{P0}\,(1 + k_x\,x + k_z\,z), \qquad (29)$$

$$Q_{P0}(x,z) = Q^{(0)}_{P0}\,(1 + j_x\,x + j_z\,z), \qquad (30)$$

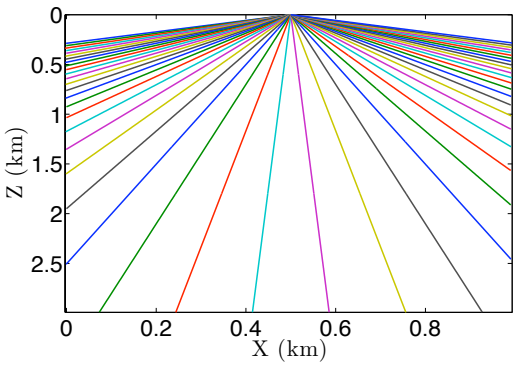

(a)

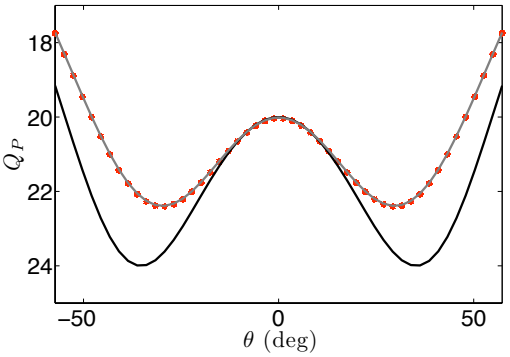

(b)

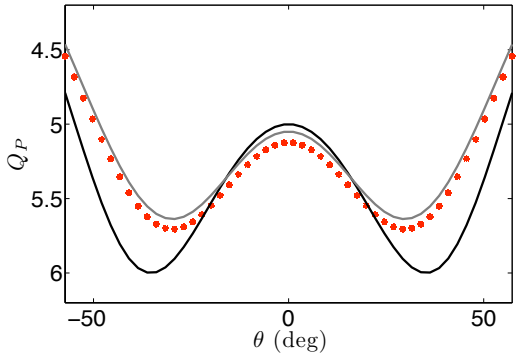

(c)

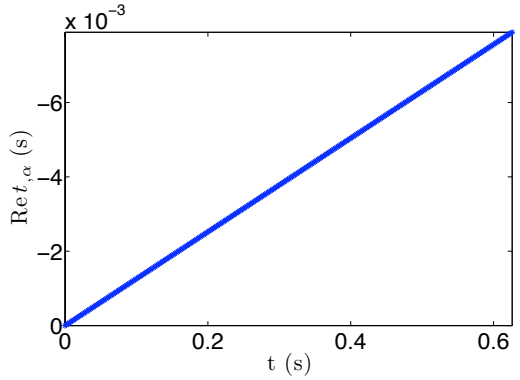

(d)

Figure 1. Ray-tracing results for models 1 and 2 from Table 1. (a) Ray trajectories. The quality factor Q_P as a function of phase angle for (b) model 1 and (c) model 2. The exact coefficient is plotted in gray, the red stars denote the value obtained from equation 27, and the black line is the linearized quality factor obtained using equation 28. (d) Perturbation of the real-valued traveltime as a function of the unperturbed traveltime computed along the ray with a take-off phase angle of 18° in model 2.

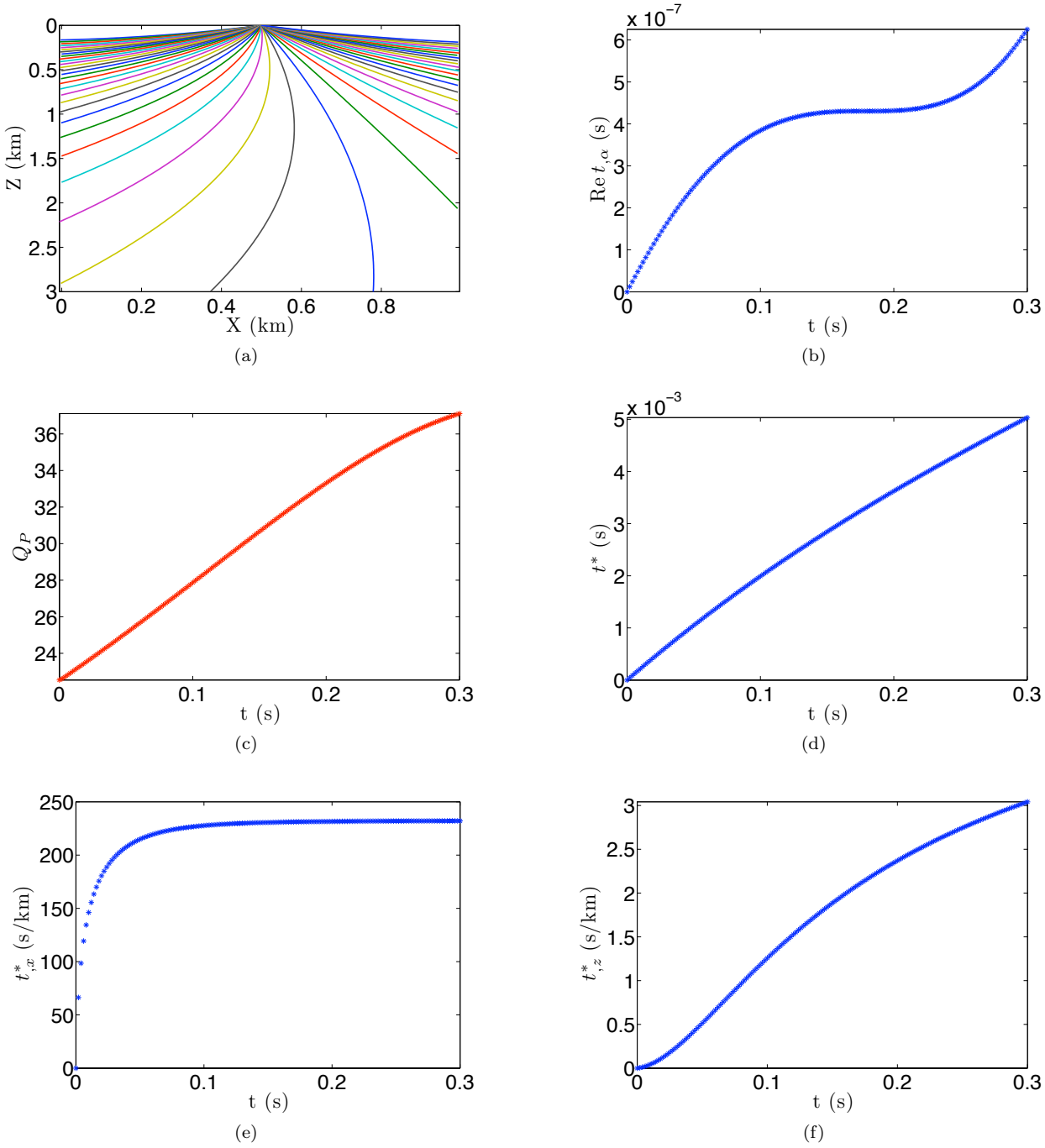

Figure 2. Ray-tracing results for model 3 from Table 1. (a) Ray trajectories. (b) Perturbation of the real-valued traveltime as a function of the unperturbed traveltime along the ray. (c) The quality factor Q_P, (d) dissipation factor t^*, and the spatial derivative of the dissipation factor with respect to (e) x and (f) z computed along the ray with a take-off phase angle of 18°.

where $V_{P0}^{(0)} = V_{P0}(x = 0, z = 0)$ and $Q_{P0}^{(0)} = Q_{P0}(x = 0, z = 0)$. Three sets of the velocity and attenuation parameters used in the tests are listed in Table 1. Models 1 and 2 are homogeneous, while model 3 has linearly varying parameters V_{P0} and Q_{P0} defined by equations 29 and 30. Figure 1a shows a fan of rays with a constant increment in the take-off phase angle from a point source for models 1 and 2. The elastic reference medium for models 1 and 2 is the same, and hence the ray trajectories for the two models coincide. There is a good agree-

Model	1	2	3
$V_{P0}^{(0)}$ (km/s)	3.00	3.00	3.00
$V_{S0}^{(0)}$ (km/s)	1.50	1.50	1.50
ϵ	0.10	0.10	0.10
δ	0.20	0.20	0.20
k_x (km^{-1})	0	0	0.20
k_z (km^{-1})	0	0	0.80
$Q_{P0}^{(0)}$	20	5	20
$Q_{S0}^{(0)}$	20	5	20
ϵ_Q	0.50	0.50	0.50
δ_Q	-1.0	-1.0	-1.0
j_x (km^{-1})	0	0	0.1
j_z (km^{-1})	0	0	1

Table 1. TI models used to test the algorithm. Models 1 and 2 are homogeneous, while model 3 has linearly varying P-wave vertical velocity V_{P0} and vertical quality factor Q_{P0}.

ment between the ray-traced and exact quality factors, even for the strongly attenuative model 2 (Figures 1b and 1c). While the linearized quality factor computed from equation 28 does not differ significantly from the exact quality factor for model 1, the deviation is more pronounced for model 2. Hence, the linearized approximation can be used in the inverse problem for moderately attenuative models. For homogeneous media, the quality factor can also be found from the dissipation factor (equation 12) and the real-valued traveltime:

$$\frac{1}{2Q} = \frac{t^*}{\mathrm{Re}\,\tau}\,. \tag{31}$$

The attenuation-induced perturbation of the real-valued traveltime (equation 22) is significant (on the order of milliseconds) only for strongly attenuative media (model 2, Figure 1d).

Figure 2a displays ray trajectories for model 3, in which V_{P0} and Q_{P0} vary linearly with x and z (Table 1). The perturbation of the real-valued traveltime due to attenuation is almost negligible (Figure 2b). Figures 2c and 2d display the P-wave quality (equation 27) and dissipation (equation 12) factors as a function of the traveltime along the ray. The spatial derivatives of the dissipation factor (Figures 2e and 2f) do not vanish, as expected for this heterogeneous model.

Basic elements of inversion methodology

Due to numerous complications involved in attenuation estimation, robust attenuation analysis typically

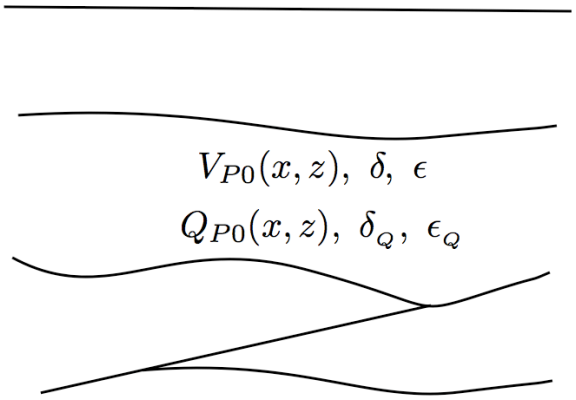

Figure 3. 2D model for velocity and attenuation estimation. The subsurface is divided into factorized blocks with VTI symmetry for both velocity and attenuation. The P-wave vertical velocity and quality factor are assumed to vary linearly with depth and lateral position, while the velocity-anisotropy parameters ϵ and δ and the attenuation-anisotropy parameters ϵ_Q and δ_Q within each block are constant.

requires the subsurface structure to be relatively simple. If the overburden is laterally homogeneous and has a horizontal symmetry plane, anisotropic attenuation coefficients of P- and S-waves can be estimated without knowledge of the velocity field using the layer-stripping method of Behura and Tsvankin (2009a) and Shekar and Tsvankin (2011). It should be mentioned that the attenuation-layer stripping method yields attenuation coefficients corresponding to a given source-receiver offset or group angle. To invert for attenuation-anisotropy parameters, it is necessary to estimate the corresponding phase angle, which requires knowledge of an approximate velocity model. However, for more complicated, heterogeneous subsurface models, attenuation estimation requires an accurate velocity field, even if the medium is isotropic.

Velocity estimation in heterogeneous anisotropic media is an active field of research (e.g., Tsvankin and Grechka, 2011). Sarkar and Tsvankin (2004) introduce a 2D method to estimate the P-wave velocity field in VTI media via migration velocity analysis (MVA). They divide the subsurface into factorized VTI blocks, in which the ratios of the stiffness coefficients and, consequently, the parameters ϵ and δ are constant. The P-wave vertical velocity in each block is assumed to vary linearly with depth and lateral position (see equation 29). Their MVA algorithm is an iterative two-step procedure that consists of Kirchhoff prestack depth migration followed by velocity updating. In the velocity-analysis step, the residual moveout is estimated in common-image gathers by a 2D semblance scan that takes long-spread (nonhyperbolic) moveout into account. The parameters of each factorized block are updated by minimizing the variance of the migrated depths. The methodology of Sarkar and

Tsvankin (2004) helps resolve the vertical and lateral velocity gradients along with ϵ and δ, provided that the velocity V_{P0} is known at a single point in each block.

To reconstruct the block-based spatially varying attenuation coefficient, we consider factorized VTI models for both velocity and attenuation (Figure 3). Within each factorized block, the velocity-anisotropy parameters as well as the attenuation-anisotropy parameters are constant, while the P-wave vertical velocity $V_{P0}^{(0)}$ and vertical quality factor $Q_{P0}^{(0)}$ vary linearly with depth and lateral position (equations 29 and 30). The kinematics of P-waves are practically independent of the attenuation coefficient for most subsurface models, except for rocks that exhibit uncommonly strong attenuation (e.g., those saturated with heavy oil, Behura et al., 2007). Therefore, the velocity field can be reconstructed using the algorithm of Sarkar and Tsvankin (2004).

The initial values of the attenuation coefficient for the top layer will be found by applying the spectral-ratio method to pairs of traces of reflections from the layer's bottom. The layer-stripping method of Behura and Tsvankin (2009a) will then be used to estimate the initial attenuation coefficients in the other layers or blocks. Since the assumptions of that method are not satisfied for models with laterally heterogeneous overburden (Figure 3), it will yield only approximate attenuation coefficients. A gradient-based inversion methodology will then be employed to refine the attenuation estimates. Since the ray-tracing algorithm described above produces the Fréchet derivatives of the complex-valued traveltime along the ray, it can be efficiently used for gradient computation.

Summary

Dynamic ray tracing represents a computationally efficient tool to calculate asymptotic Green's functions in attenuative anisotropic media. Here, we implemented the algorithm of Červený and Pšenčik (2009), which relies on ray perturbation theory, to model P-wave amplitudes for 2D heterogeneous attenuative VTI media. The attenuation-related terms are computed as perturbations of the reference quantities along rays traced in an elastic background medium. This technique also produces the Frèchet derivatives of the Green's function, which can be used in solving the inverse problem. We tested the ray tracing methodology on TI models with constant as well as laterally varying velocity and attenuation functions. The algorithm produces accurate P-wave traveltimes and attenuation coefficients, even for models with extremely strong attenuation. The examples also show that the influence of attenuation on traveltime is significant only for media with an uncommonly small quality factor.

Attenuation estimation in heterogeneous TI media has to be preceded by accurate reconstruction of the velocity field. Since attenuation induced traveltime changes are typically negligible, we proposed to perform velocity estimation using the migration velocity analysis (MVA) algorithm of Sarkar and Tsvankin (2004) for piecewise-factorized VTI media. The attenuation coefficients in each factorized block can be represented as linear functions of the spatial coordinates and obtained by gradient-based inversion. The perturbation ray-tracing method substantially reduces the cost of modeling and provides essential quantities for the inversion operator.

Acknowledgments

We are grateful to the members of the A(nisotropy)-Team of the Center for Wave Phenomena (CWP), Colorado School of Mines, for fruitful discussions. Bharath Shekar wishes to acknowledge John Stockwell (CWP) and Sribharath Kainkaryam (Purdue) for their help with ray-theory concepts. Support for this work was provided by the Consortium Project on Seismic Inverse Methods for Complex Structures at CWP and by the Research Partnership to Secure Energy for America (RPSEA).

REFERENCES

Behura, J., M. Batzle, R. Hofmann, and J. Dorgan, 2007, Heavy oils: Their shear story: Geophysics, **72**, no. 5, E175–E183.

Behura, J., and I. Tsvankin, 2009a, Estimation of interval anisotropic attenuation from reflection data: Geophysics, **74**, no. 6, A69–A74.

———, 2009b, Role of the inhomogeneity angle in anisotropic attenuation analysis: Geophysics, **74**, no. 5, WB177–WB191.

Brzostowski, M. A., and G. A. McMechan, 1992, 3-D tomographic imaging of near-surface seismic velocity and attenuation: Geophysics, **57**, 396–403.

Carcione, J., 1990, Wave propagation in anisotropic linear viscoelastic media: theory and simulated wavefields: Geophysics Journal International, **101**, 739–750.

———, 2011, A generalization of the Fourier pseudospectral method: Geophysics, **76**.

Červený, V., 2001, Seismic ray theory: Cambridge University Press.

Červený, V., and I. Pšenčik, 2005, Plane waves in viscoelastic anisotropic media – I. Theory: Geophysics Journal International, **161**, 197–212.

———, 2009, Perturbation Hamiltonians in heterogeneous anisotropic weakly dissipative media: Geophysics Journal International, **178**, 939–949.

Dewangan, P., and I. Tsvankin, 2006, Velocity-independent layer stripping of PP and PS reflection traveltimes: Geophysics, **71**, no. 4, U59–U65.

Gajewski, D., and I. Pšenčik, 1992, Vector wavefield for weakly attenuating anisotropic media by the ray method: Geophysics, **57**, 27–38.

Hanyga, A., and M. Seredyňska, 2000, Ray tracing in elastic and viscoelastic media: Pure and Applied Geophysics, **157**, 679–717.

Johnston, D. H., and M. Toksöz, 1981, Seismic wave attenuation: Society of Exploration Geophysicists. Geophysics reprint series.

Kjartannson, E., 1979, Constant Q-Wave Propagation and Attenuation: Journal of Geophysical Research, **84**, 4737–4748.

Liao, Q., and G. A. McMechan, 1997, Tomographic imaging of velocity and Q, with application to cross-well seismic data from the Gypsy Pilot Site Oklahoma: Geophysics, **62**, 1804–1811.

Lynn, H. B., 2004, The winds of change: Anisotropic rocks-their preferred direction of fluid flow and their associated seismic signatures-Part 1: The Leading Edge, 1156–1162.

Menke, W., 1984, Geophysical data analysis: discrete inverse theory, volume 45 of International Geophysical Series: Academic Press.

Moser, T. J., and V. Červený, 2009, Paraxial ray methods in inhomogeneous anisotropic media: initial conditions: Studia Geophysica etc Geodaetica, **53**, 199–214.

Quan, Y., and J. M. Harris, 1997, Seismic attenuation tomography using the frequency shift method: Geophysics, **62**, 895–905.

Reine, C. A., R. A. Clark, and M. van der Baan, 2009, Interval-Q Measurements from Surface Seismic Data Using a Robust Prestack Inversion Algorithm: 71st EAGE Conference & Exhibition.

Ruud, B. O., and S. Hestholm, 2005, Modeling seismic waves in orthorhombic, viscoelastic media by finite-differences: 75th Annual International Meeting, SEG, Expanded Abstracts.

Sarkar, D., and I. Tsvankin, 2004, Migration velocity analysis in factorized VTI media: Geophysics, **69**, 708–713.

Schmidt, H., and G. Tango, 1986, Efficient global matrix approach to the computation of synthetic seismograms: Geophysical Journal of the Royal Astronomical Society, **84**, 331–359.

Shekar, B., and I. Tsvankin, 2011, Estimation of shear-wave interval attenuation from mode-converted data: Geophysics, **76**, no. 6, D11–D19.

Thomson, C. J., 1997, Complex rays and wave packets for decaying signals in inhomogeneous, anisotropic and anelastic media: Studia Geophysica etc Geodaetica, **41**, 345–381.

Tsvankin, I., and V. Grechka, 2011, Seismology of azimuthally anisotropic media and seismic fracture characterization: SEG.

Xin, K., B. Hung, S. Birdus, and J. Sun, 2008, 3-D tomographic amplitude inversion for compensating amplitude attenuation in the overburden: 78th Annual International Meeting, SEG, Expanded Abstracts, 3239–3243.

Xu, T., and G. A. McMechan, 1998, Efficient 3-D viscoelastic modeling with application to near-surface land seismic data: Geophysics, **63**, 601–612.

Zhu, Y., and I. Tsvankin, 2006, Plane-wave propagation in attenuative transversely isotropic media: Geophysics, **71**, no.2, T17–T30.

Zhu, Y., I. Tsvankin, P. Dewangan, and K. V. Wijk, 2007, Physical modeling and analysis of P-wave attenuation anisotropy in transversely isotropic media: Geophysics, **72**, no. 1, D1–D7.